

Proteomic characterization reveals CYP2S1 as a mediator of drug resistance in PDAC

Vera Thiel, PhD<sup>1, 2,†</sup>, Wiebke M. Nadler, PhD <sup>1,2,\*,†</sup> Alexander Kerner, PhD<sup>1, 2</sup>, Laura Kuhlmann, PhD<sup>1, 2, 3</sup>, Manuel Reitberger, PhD<sup>1, 2</sup>, Tim Vorberg<sup>1, 2</sup>, Paul Schwerd-Kleine<sup>1, 2</sup>, Elisa Noll, PhD<sup>1</sup>, Nathalia A. Giese, MD, Hsi-Yu Yen, Dr. med. vet., <sup>5, 7, 8</sup>, Katja Steiger, Dr. med. vet., Vanessa Vogel<sup>1, 2,9</sup>, Corinna Klein<sup>1, 2</sup>, Thilo Hackert, MD<sup>4</sup>, Ronald Koschny, MD<sup>6</sup>, Christiane A. Opitz, PhD<sup>1</sup>, Andreas Trumpp, PhD<sup>1, 2</sup>, Martin R. Sprick, PhD <sup>1,2,‡\*</sup> and Christoph Rösli, PhD <sup>1,2,‡</sup>

- German Cancer Research Center (DKFZ), Heidelberg, Germany;
- <sup>2</sup> HI-STEM gGmbH, Heidelberg, Germany;
- National Cancer Institute, Rockville, MD, USA;
- Department of General and Visceral Surgery, University Hospital Heidelberg, Heidelberg, Germany;

- Institute of Pathology, School of Medicine, Technical University of Munich, Germany;
- Department of Internal Medicine IV, Interdisciplinary Endoscopy Center, University Hospital Heidelberg, Heidelberg, Germany;
- <sup>7</sup> German Cancer Consortium (DKTK), Partner Site Munich;
- 8 Current address: Bayer Research and Development, Wuppertal, Germany;
- <sup>9</sup> Current address: Department of Pathology, University Hospital Heidelberg, Germany;
- † These authors contributed equally to this work.
- ‡ These authors contributed equally to this work.
- \* Co-corresponding authors

Address for correspondence: martin.sprick@hi-stem.de, wiebke.nadler@philipa.de

Dr. Martin Sprick

DKFZ Heidelberg/HI-STEM

Im Neuenheimer Feld 280

69120 Heidelberg, Germany

martin.sprick@hi-stem.de

## Financial support:

This work was in part supported by the Dietmar Hopp Foundation, the BioRN Spitzencluster "Molecular and Cell based Medicine", the German Ministry of Science and Education (BMBF) e:Med program for systems biology (PANC-STRAT consortium, grant no. 01ZX1305C and 01ZX1605C; A), the DKFZ-NCT program NCT3.0, and the German Cancer Consortium (DKTK) Joint Funding Program. KS and WW received funding from DFG (Both: SFB1321, project number: 329628492; S01, WW: CRC1321). We thank the NCT Molecular Precision Oncology Program for technical support and funding through project

numbers HIPO-015 and HIPO-K20K. Provision of the pancreatic samples was supported by the Pancobank – a Biobank of the European Pancreas Center at the Department of General, Visceral and Transplantation Surgery, University Hospital Heidelberg. Chaired by Prof. Dr. M.W. Büchler, the Pancobank is affiliated with the German Biobank Alliance through a membership in the BioMaterialBank Heidelberg (BMBH)-Consortium led by Prof P. Schirmacher (BMBF grants 01EY1101 and GBA/BBMRI.de: 01EY1707).

Running title:Role of CYP2S1 in PDAC drug resistance

#### **Abstract:**

**Objectives:** To investigate the proteomic profile of different molecular subtypes of pancreatic ductal adenocarcinoma (PDAC) and understand their impact on patient outcomes, particularly focusing on pathways involved in xenobiotic metabolism and drug resistance.

Methods: The study utilized the serum-free PACO cell culture model and a quantitative prefractionation-based MALDI/MS approach to establish the proteomic profiles of various PDAC subtypes. Differential protein regulation was analyzed to identify systematic alterations in metabolic and drug resistance pathways. Mechanistic studies involved the knockdown and overexpression of key proteins to assess their role in drug resistance.

**Results:** Proteomic analysis revealed subtype-specific alterations, particularly in pathways associated with xenobiotic metabolism and drug resistance. Notably, CYP2S1, a member of the CYP450 family, was upregulated in the HNF1A+ PDAC subtype. CYP2S1 levels were further inducible by polyaromatic hydrocarbons (PAHs) and SN38, the active metabolite of

irinotecan via AHR. Mechanistic studies demonstrated that knockdown of AHR or CYP2S1 sensitized PDAC cells to SN38, whereas overexpression of CYP2S1 increased resistance to SN38.

Conclusions: The findings highlight the significant role of CYP2S1 in mediating drug resistance in certain PDAC subtypes. Targeting CYP2S1 and its regulatory pathways could enhance the efficacy of chemotherapeutic agents like irinotecan in treating PDAC. These results provide new insights into the molecular mechanisms underlying PDAC subtypespecific drug resistance and suggest potential therapeutic targets.

Keywords: AHR; CYP2S1; GeLC-based MALDI/MS; MSQBAT; PDAC

#### Introduction

Pancreatic ductal adenocarcinoma (PDAC) accounts for > 85% of pancreatic cancer cases and is the fourth most frequent cause of cancer death in the western world <sup>1, 2</sup>. Current therapies offer only modest benefits to the patients suffering from PDAC: Among patients with resected PDAC, adjuvant therapy with a modified FOLFIRINOX scheme (folinic acid, fluorouracil, irinotecan and oxaliplatin) or gemcitabine resulted in a median overall survival of 54.4 months and 35.0 months, respectively <sup>3</sup>. Although extensive research has been carried out, high intrinsic or acquired resistance to chemotherapy complicates attempts to improve the available therapeutic approaches.

In 2011, Collisson and co-workers defined three different subtypes of PDAC based on gene expression profiling of laser-micro-dissected primary tumors, which they termed a) classical, b) quasi-mesenchymal and c) exocrine-like <sup>4</sup>. To facilitate stratification in a clinical setting, Noll *et al.* later suggested HNF1A and KRT81 as surrogate markers for these three subtypes, thereby distinguishing a) HNF1A-/KRT81-, b) KRT81+ and c) HNF1A+ tumors <sup>5</sup>. Based on this stratification scheme, significant differences in overall survival were observed for the subtypes in a cohort of 217 patients. Alternative classifications based on transcriptomic, genomic or epigenetic features exist and can be used to robustly separate PDAC into clinically relevant subtypes <sup>6,8,9</sup>. Further information on the overlap between the classifications can be found in <sup>10</sup> and <sup>11</sup>.

Considerable efforts have been made to achieve a comprehensive picture of the PDAC proteome <sup>12</sup>. Although impressive progress has been published recently, the acquisition of accurate proteomic information from PDAC patient samples remains challenging due to the extensive stromal component of this cancer type <sup>9, 10</sup>. Noll, Eisen and colleagues therefore established the PACO (**P**ancreatic **A**deno**C**arcin**O**ma) model system for the cultivation of

primary PDAC cell lines <sup>5</sup>. In brief, the PACO model cell lines were generated by orthotopic transplantation of PDAC patient samples into NSG mice. Following engraftment, resulting xenotransplants were dissociated into single cells and established as *in vitro* culture using a chemically defined culture medium. Upon transplantation of the cultured PACO cells into secondary recipient NSG mice, histopathology of resulting tumors closely resembled the initial patient sample <sup>5</sup>.

These PACO model cell lines were used as the basis for the in-depth analysis of differences in protein expression between PDAC subtypes presented here. To the best of our knowledge, this is the largest proteome dataset that has ever been quantified using a MALDI-based MS approach.

A major finding of this first part of our study relates to systematic alterations of pathways involved in xenobiotic metabolism and drug resistance as a function of the PDAC subtype. Various mechanisms of drug resistance have been proposed for PDAC, such as microenvironment-induced reprogramming, extensive tumor stroma acting as a drug barrier, or changes in signaling and gene expression profiles <sup>13</sup>. In particular, increased levels of certain drug-metabolizing enzymes appear to influence the efficiency of therapeutic agents <sup>14</sup>. Members of the cytochrome P450 protein family have been described to catalyze a variety of oxidative, peroxidative and reductive reactions on a broad range of substrates, including procarcinogens and pro-mutagens. Increased CYP450 protein levels can however also influence the pharmacokinetics of therapeutic agents, as demonstrated in PDAC for CYP3A5 which mediates the metabolism of small molecule tyrosine kinase inhibitors and paclitaxel <sup>5</sup>. In the second part of our investigations, we evaluated the functional relevance of CYP2S1 for drug resistance in PDAC, an orphan CYP450 protein that was heavily upregulated in the HNF1A+ subtype according to our large-scale proteomic study. In the context of cancer, CYP2S1 expression is associated with poor prognosis e.g. for colorectal carcinoma <sup>15</sup> and has

recently been described as synthetic lethal target in BRAF V600E-driven thyroid cancers <sup>16</sup>. Interestingly, CYP2S1 can be induced by various pro-carcinogenic polyaromatic hydrocarbons (PAHs) in PDAC. Furthermore, we could unexpectedly uncover that CYP2S1 is not only inducible by SN38 (7-Ethyl-10-hydroxycamptothecin), but also mediates resistance to SN38 in PDAC cells with endogenous expression of CYP2S1. SN38 is the active metabolite of cancer drug irinotecan and is generated by carboxylesterases (CES) mediated hydrolysis <sup>17</sup>. SN38 then targets topoisomerase I, thereby inhibiting DNA replication in cancer cells and ultimately leading to their death <sup>18</sup>.

#### **Material and Methods**

# **Experimental Design and Statistical Rationale**

An overview of the prefractionation-based label-free MALDI/MS quantification approach is depicted in Figure 1a, while the detailed description can be found in SI Section III, Supplemental Digital Content 1, http://links.lww.com/MPA/B412. In brief, at least three cell lines per PDAC subtype (i.e. three biological replicates, see Table S1b, Supplemental Digital Content 2, http://links.lww.com/MPA/B413) and control cell lines HPDE and HPNE (i.e. two biological replicates) were grown to 80% confluence in their respective medium and were subsequently washed and lysed on flask. Separation of the lysate by SDS-PAGE was monitored by Coomassie staining to facilitate the manual execution of a complex slice-and-pool algorithm designed to ensure uniform protein complexity per fraction. The resulting twelve gel fractions per cell line were destained, and cysteine residues were reduced and carbamidomethylated to circumvent artifacts from disulfide bridges. Proteins in the gel slices were subjected to tryptic digest and resulting peptides were extracted from the gel. After desalting, peptide mixtures were subsequently separated using nanoflow ultra-high-performance liquid chromatography (UHPLC, C18 nanoAcquity UPLC Column; 75 µm x 250 mm; 1.7 µm BEH130, Waters). Eluting peptides were mixed with alpha-Cyano-4-

hydroxycinnamic acid matrix comprising four spike-in peptides to standardize quantification, and were automatically deposited on stainless steel plates (600 spots per gel fraction). A MALDI TOF/TOF 5800 mass spectrometer (SCIEX) was used for the analysis of the samples. Following acquisition of the MS data, a maximum of 35 precursors per fraction was selected for MS/MS. Spectra from each individual LC-run were searched against a human reference proteome database containing 70101 protein entries from Swiss-Prot and trEMBL using the Paragon algorithm (ProteinPilot). Prior to quantification, peptides were classified as proteotypic, degenerated or not found using PepSir software. For quantification, peak lists from MS raw spectra were extracted and loaded into MSQBAT, along with the identifications of the proteotypic peptides. The automated complexity reduction performed during this step dismissed 50 to 70% of all features per gel fraction. To compensate for inter-sample variation of the MALDI laser intensity, samples were subjected to a global normalization step performed with respect to each cell line. The genetic algorithm implemented in MSQBAT was applied to find the optimal combination of settings for a robust alignment. By aligning the matching gel fractions of all cell lines, twelve different super-alignments were prepared, i.e., one per gel fraction. Each gel fraction of a cell line was then aligned with the respective super-alignment. After summing up the peptide intensities for each protein, the protein ratios were computed and subsequently factorized to obtain intensity-like values for data analysis. For principal component analysis (PCA) and hierarchical clustering, glog2 transformed protein quantification data and additional information on subtype and patient were combined in an R expression set object. Proteins with missing values (~20%) were excluded from the analysis and the remaining data were normalized using the vsn package. Differentially expressed proteins were retrieved from the VSN normalized data set using the limma package.

### **Cell lines and Samples**

Human pancreatic nestin-expressing (HPNE <sup>19</sup>) and human pancreatic ductal epithelial (HPDE <sup>20</sup>) cells (ATCC) were cultured according to the supplier's instructions. PACO cell lines were cultured under serum-free conditions without antibiotics as described by Noll *et al.*<sup>5</sup> (see SI Section I, Supplemental Digital Content 1, http://links.lww.com/MPA/B412). Tissue samples were obtained from patients who received partial pancreatoduodenectomy at the Department of General, Visceral and Transplantation Surgery, University of Heidelberg (see SI Section II, Supplemental Digital Content 1, http://links.lww.com/MPA/B412). The studies were approved by the ethical committee of the University of Heidelberg (case numbers S-206/2011, S-161/2007, S-551/2012 and EPZ-Biobank Ethic Votes #301/2001, S-976/2020, S-083/2021) and conducted in accordance with the Helsinki Declaration. All cell lines were authenticated by a SNP test (SNP Typing, Multiplexion, Heidelberg, Germany) and compared with reference SNP profiles obtained from the primary patient material. Cell lines were regularly tested for mycoplasma contamination (Contamination Test, Multiplexion, Heidelberg, Germany).

## **Multiple reaction monitoring**

Cultured cells or snap frozen tissue samples were lysed and samples with equal protein amounts were used as input material for multiple reaction monitoring (MRM) using a QTRAP 6500 system equipped with a TurboV ion source (SCIEX) and coupled online to a nanoAcquity UHPLC system (Waters), see SI Section IV, Supplemental Digital Content 1, http://links.lww.com/MPA/B412 for details.

## **Xenograft Staining**

PACO cells were injected into the pancreas of immune-deficient NSG mice as described in <sup>5</sup> (see SI Section V, Supplemental Digital Content 1, http://links.lww.com/MPA/B412).

Derived tumors were harvested and fixed in formaldehyde to obtain secondary xenograft

sections. Immunohistochemistry staining was performed using rabbit polyclonal anti-human-AHR antibody (sc-5579, Santa Cruz) or rabbit polyclonal anti-human-CYP2S1 antibody (ab69650, Abcam).

Animals were bred in the animal facility of the German Cancer Research Center and animal care and all procedures were previously approved by the governmental review board of the state of Baden-Wuerttemberg, Regierungspraesidium Karlsruhe (authorization numbers G39-13, G305-14 and G80-15).

#### Tissue microarray (TMA)

The TMA was constructed from pancreatic specimens as described in SI Section VI, Supplemental Digital Content 1, http://links.lww.com/MPA/B412, while processing and evaluation including subtyping, was performed as described in <sup>21</sup>. Semiquantitative scoring of the CYP2S1 immunohistochemistry (ab69650, Abcam) was performed with respect to cytoplasmic positivity, with slight expression in fewer than 30% of tumor cells defined as low and slight or moderate expression in more than 30% of tumor cells as high.

### **Immunofluorescence**

In brief, PACO cells were cultured on cell culture inserts for 72 hours before the respective compound was added, see SI Section VII, Supplemental Digital Content 1, http://links.lww.com/MPA/B412. Rabbit polyclonal anti-human-AHR antibody (HPA029723, Sigma) or rabbit polyclonal anti-human-CYP2S1 antibody (ab69650, Abcam) were used as primary antibodies. Samples were analyzed with an LSM 700 confocal laser scanning microscope operated with LSM 700 Axio Imager 2 software (Zeiss).

#### **Induction assays**

PACO cells were grown for 48 hours, before fresh medium comprising the respective compound was added, i.e. β-Naphthoflavone (bNF, MFCD00004985, Sigma), 3-

Methylcholanthrene (3MC, 56-49-5, Sigma), Benzo[a]pyrene (BaP, 50-32-8, Sigma), 2,3,7,8-Tetrachlorodibenzo-p-dioxin (TCDD, ARCD0413, American RadiolabeledChemicals Inc.), AhR Inhibitor (Merck Millipore, 182706-5MG), SN-38 (SN-38 glucuronide, 121080-63-5, Santa Cruz) or topotecan (topotecan hydrochloride, sc-204919, Santa Cruz). After incubation cells were washed and subjected to further analysis.

## Real-time quantitative PCR

Total RNA was extracted using the miRNeasy mini kit (Qiagen) and reverse transcribed using the high capacity cDNA reverse transcription kit (Applied Biosystems). cDNA corresponding to 10 ng of starting RNA was used for relative RNA quantification (qRT-PCR). TaqMan probes (Applied Biosystems) for CYP2S1 (Hs00258076\_m1), TIPARP (Hs00296054\_m1), AHR (Hs00907314\_m1), HNF4A (Hs00230853\_m1) and GAPDH (HS9999905\_m1) were used to acquire expression data with the Viia 7 Real-Time PCR System (Applied Biosystems) operated with ViiA 7 software 1.1.

### Generation of stable knockdown cells

The CYP2S1 or AHR shERWOOD UltramiR shRNA Lentiviral Target Gene Set was used in pZIP-mCMV-ZsGreen vector (BioCat) for stable knockdown of CYP2S1 or AHR. A detailed description can be found in SI Section IX, Supplemental Digital Content 1, http://links.lww.com/MPA/B412.

### Stable expression of CYP2S1

PACO cells were stably transduced with the expression vector iTd2 Tomato plasmid containing the full CYP2S1 open reading frame, or with empty vector control, see SI Section X, Supplemental Digital Content 1, http://links.lww.com/MPA/B412.

### **Drug treatment assays**

PACO cells were seeded into 96-well plates and fresh medium with SN-38 (Glucuronide, 121080-63-5, Santa Cruz) was added after 24 hours. The respective concentrations were prepared in quadruplicates using 1:4 serial dilutions. Cell toxicity was analyzed using CellTox Green (Promega) after 24, 48 and 72 hours. After incubation for 72 hours, cell viability was furthermore assessed using CellTiterBlue (Promega) according to the manufacturer's instructions. In the alternative, cell proliferation was assessed using the CrystalViolet Assay (Sigma), see SI Section XI, Supplemental Digital Content 1, http://links.lww.com/MPA/B412 for a detailed description.

#### siRNA transfection of PACO cells

HNF4A siRNA or non-targeting siRNA (NT-control) (On-Target plus SMARTpool, Thermo Scientific) were used with Dharmafect 4 for the transfection of PACO cells, see SI Section XII, Supplemental Digital Content 1, http://links.lww.com/MPA/B412.

#### **AHR-ligand assay**

HEK293T cells were transfected with AHR, ARNT and Cignal xenobiotic response element (XRE)-GFP reporter (Qiagen) plasmids using FuGENE HD (Promega) according to the manufacturer's instructions, see SI Section XIII, Supplemental Digital Content 1, http://links.lww.com/MPA/B412.

#### **Results**

## Expression of biotransformation enzymes in the HNF1A+ PDAC subtype

The proteome of twelve primary patient-matched PDAC (PACO) and two control cell lines (HPDE, HPNE) was analyzed using a prefractionation-based label-free MALDI/MS approach (**Figure 1a**). The in-house quantification software MSQBAT <sup>22</sup> enabled the quantification of more than 4900 proteins (out of 5626 identified proteins) in all cell lines based on proteotypic peptides. The resulting data set with glog2 transformed, VSN-normalized data is provided as

a data resource in Table S1, Supplemental Digital Content 2, http://links.lww.com/MPA/B413.

In the absence of any information regarding subtype, explorative analysis of the protein data set using principal component analysis (PCA) (**Figure 1b**) or hierarchical clustering (Figure S2a, Supplemental Digital Content 1, http://links.lww.com/MPA/B412) separated the cell lines into three different groups. Annotation of the cell lines according to the stratification scheme suggested by Noll *et al.* <sup>5</sup> (**Figure 1b**) revealed that the control cell lines and the HNF1A+ subtype had formed separate groups, while the HNF1A-/KRT81- as well as the KRT81+ cell lines were combined in the third cluster, suggesting a higher degree of similarity of the last two subtypes on proteomic level.

In a second step, the available subtype information according to Noll *et al.* was applied to group the samples (Figure S1b, Supplemental Digital Content 1,

http://links.lww.com/MPA/B412, Table S1b, Supplemental Digital Content 2,

http://links.lww.com/MPA/B413), and linear models were used to assess differential protein expression between these groups (**Figure 1c**). The combined set of proteins with significant differences between at least two groups was retrieved (BH adj. p value < 0.05, 310 proteins, Table S2, Supplemental Digital Content 2, http://links.lww.com/MPA/B413), and was subsequently subjected to protein interaction and enrichment analysis using the string protein tool <sup>23</sup>. This analysis revealed significant alterations of pathways involved in xenobiotic metabolism and drug resistance as a function of the tumor subtype (**Figure 1d.** S1a, Supplemental Digital Content 1, http://links.lww.com/MPA/B412).

Proteins with a known role in xenobiotic transformation (i.e. metapathway biotransformation phase I and II, see <sup>24</sup>) were retrieved from the set of quantified proteins, heatmaps were generated for the respective protein families, and protein families were arranged according to their function (**Figure 2a**). Interestingly, AKR1B10, CES2, CYP2S1, GPX2, GSR, HNMT,

MAOB, UGT1A10 and UGT1A6 were significantly upregulated in the HNF1A+ PDAC subtype.

PCA and hierarchical clustering using only proteins with a known role in xenobiotic transformation as variables robustly separated the HNF1A+ subtype from the other samples (Figure S2b, S2c, Supplemental Digital Content 1, http://links.lww.com/MPA/B412), suggesting major differences in the clearance of various compounds, such as chemotherapeutic agents between the subtypes.

To validate these findings, whole cell lysates of three HNF1A+ PACO cell lines, of pancreatic tissue samples and of liver tissue samples were prepared, and protein levels of previously detected biotransformation enzymes were quantified using multiple reaction monitoring (MRM) (Table S3a-c, S4, Supplemental Digital Content 2, http://links.lww.com/MPA/B413), Interestingly, with regard to these enzymes, the HNF1A+ PDAC cell lines showed a higher similarity with liver tissue than with pancreatic tissue

Cytochrome P450 member CYP2S1 was identified among the proteins with the most prominent differential expression between subtypes and was therefore selected for further functional characterization as a candidate for drug detoxification in the HNF1A+ PDAC subtype.

## **CYP2S1** expression in the HNF1A+ PDAC subtype

(Figure 2b).

Further validation experiments using MRM confirmed the differential expression of CYP2S1 in the PDAC subtypes, and revealed a comparatively low protein expression level in full lysates of normal pancreas or normal liver (**Figure 2e**). Consistent with the previous findings, immunostainings on HNF1A+ xenograft sections showed a strong staining of CYP2S1 (**Figure 2c, left panel**).

To evaluate CYP2S1 expression also in PDAC patients, 164 patient biopsies with known subtype annotation were stained (Figure S3h, Supplemental Digital Content 1, http://links.lww.com/MPA/B412). While the highest percentage of CYP2S1 high expression was observed for the HNF1A+ subtype (~52%), this percentage was only slightly lower for the HNF1A-/KRT81- subtype. In contrast, only ~31% of the samples of the KRT81+ subtype showed a high CYP2S1 expression. As we did not have detailed treatment information for the patients available, we cannot rule out that previous, CYP2S1-inducing treatments, confounded these results (**Table in** Figure S3h, Supplemental Digital Content 1, http://links.lww.com/MPA/B412).

# PAH treatment increases CYP2S1 mRNA and protein levels in PDAC cells

Because at least in some species CYP2S1 mRNA levels have been previously described to be inducible by dioxin <sup>25</sup>, it was speculated that the dioxin receptor AHR might play a role for the upregulation of CYP2S1 in HNF1A+ PDAC.

In a first step, the overall AHR expression levels were retrieved from the proteome dataset – and were found to correlate with the expression of CYP2S1 in the respective subtype: While the expression of the transcription factor AHR was very low in the control cell lines (HPDE, HPNE), it was higher in the HNF1A-/KRT81- and KRT81+ subtype and the highest in HNF1A+ PDAC (**Figure 2d,** S2d, Supplemental Digital Content 1,

http://links.lww.com/MPA/B412). Also, immunostainings of HNF1A+ xenograft sections showed a strong staining for AHR (**Figure 2c, right panel**).

To further analyse the impact of polyaromatic hydrocarbons on CYP2S1 expression in PDAC, HNF1A+ PDAC cell lines PACO10, PACO14 and PACO18 were treated for 72 hours with 2,3,7,8-tetrachlorodibenzo-p-dioxin (TCDD, "dioxin"). AHR activation was subsequently evaluated qualitatively based on AHR translocation into the nucleus (visualized

using confocal microscopy) <sup>26</sup> (**Figure 3e**), or quantitatively using mRNA expression levels of the known AHR target gene TIPARP (determined by qRT-PCR) <sup>27</sup>.

Upon TCDD treatment all three HNF1A+ PDAC cell lines showed not only a significant increase in TIPARP mRNA levels, but also a substantial increase of CYP2S1 mRNA expression (**Figure 3a**).

A time course experiment showing the increase of TIPARP and CYP2S1 mRNA levels upon TCDD treatment of PACO18 cells is depicted in **Figure 3b**. Maximum values for TIPARP were reached after 3 hours and levels remained high for at least 72 hours, while CYP2S1 mRNA peaked at approx. 48 hours.

To confirm the relevance of AHR for the hypothesized mode of CYP2S induction in PDAC, further PAHs benzo(a)pyrene (BaP), β-naphthoflavone (βNF) and 3-methylcholanthrene (3-MC) were tested for their potential to modulate TIPARP and CYP2S1 mRNA levels. The chemical structures of these PAHs are shown in **Figure 3d**. Similar to TCDD, each of these PAHs induced a significant increase in TIPARP and CYP2S1 mRNA levels in PACO10 cells (**Figure 3c**). **Figure 3e** shows a confocal staining visualizing increased levels and nuclear translocation of AHR upon TCDD or BaP treatment of PACO18 cells after 72 hours (green dots). Translocation of ligand-bound AHR from the cytosol to the nucleus is an essential event in AHR activation. For comparison: co-treatment of the cells with BaP and AHR inhibitor (AHRi) results in lower total protein levels of AHR without specific nuclear AHR accumulation.

As shown in **Figure 4** for PACO14, a substantial increase in cytoplasmic CYP2S1 protein levels can be observed by confocal microscopy upon BaP treatment. Moreover, this effect was at least partially prevented by co-administration of a small molecule antagonist of AHR (AHRi).

SN38 is a ligand of AHR and induces CYP2S1 expression in PACO cells

Irinotecan and its active metabolite SN38 inhibit the topoisomerase I enzyme and show efficacy in various tumor indications including pancreatic cancer <sup>28</sup>. Because SN38 shares certain structural similarities with polyaromatic hydrocarbons (see Figure S4g, Supplemental Digital Content 1, http://links.lww.com/MPA/B412), it was hypothesized that SN38 might likewise be a ligand of AHR and might be able to induce CYP2S1 expression. To test this hypothesis, several PDAC cell lines were treated with SN38. TIPARP and CYP2S1 mRNA levels were subsequently investigated by qRT-PCR (Figure 5a). Significant upregulation of both, TIPARP and CYP2S1 mRNA expression was observed not only in HNF1A+ PDAC cell lines PACO10, PACO14 and PACO18, but also in the two tested cell lines of the KRT81+ subtype, PACO7 and PACO19. However, the endogenous protein expression of CYP2S1 and AHR was lower in this subtype (Figure 2d/e, Figure S2d, Supplemental Digital Content 1, http://links.lww.com/MPA/B412). Two commercially available PDAC cell lines were also tested to assess the broader applicability. PANC1, classified as a Quasi-Mesenchymal (KRT81+) subtype, and CAPAN1, an Exocrine-like (HNF1A+) subtype, were chosen for this validation. Consistent with our observations in PACO cells, the exocrine-like (HNF1A+) CAPAN1 cell line exhibited higher basal CYP2S1 expression, as indicated by lower CT values in qPCR analysis (Figure S2e, Supplemental Digital Content 1, http://links.lww.com/MPA/B412). We tested CYP2S1 induction in both CAPAN1 (HNF1A+) and PANC1 (HNF1A low) cell lines following treatment with SN38. Our results showed that CYP2S1 expression was inducible in both cell lines (Figure S2e, f, Supplemental Digital Content 1, http://links.lww.com/MPA/B412). The kinetics of SN38-based TIPARP and CYP2S1 induction were found to be similar to

those observed previously for TCDD treatment in PACO cell lines (**Figure 5b**).

Finally, an AHR-ligand assay was performed using HEK293T cells, which confirmed that SN38 is a direct ligand of AHR (**Figure 5c**).

Interestingly, topotecan, another topoisomerase inhibitor and analog of SN38 also induced CYP2S1 expression, presumably via AHR as suggested by TIPARP upregulation (Figure **5d**). Both, topotecan and SN38 comprise a polyaromatic core structure, see Figure S4g, Supplemental Digital Content 1, http://links.lww.com/MPA/B412. The effects of AHR activation were analyzed on other drug-resistance related molecules including Ces2, UGT1A, UGT1A6, ABCB1, CYP3A5, ATF3, and KMO. CES2, an enzyme involved in the hydrolysis of irinotecan to its active metabolite SN38, was significantly upregulated, along with ATF3, a stress-responsive transcription factor that is a well-established downstream target of AHR. KMO (Kynurenine 3-Monooxygenase), a critical enzyme in the tryptophan metabolic pathway, was also upregulated upon SN38 treatment. This is consistent with the role of AHR in regulating genes involved in tryptophan metabolism. In contrast, CYP3A5 and the drug transporter ABCB1 did not exhibit significant changes in expression, which aligns with their known roles in the metabolism of drugs like paclitaxel, indicating specificity in the response to AHR activation and SN38 treatment. Notably, the downregulation of UGT1A isoforms, which are involved in the detoxification of SN38 through glucuronidation, suggests a potential negative feedback mechanism. These findings demonstrate that AHR activation and CYP2S1 overexpression selectively influence the expression of specific genes involved in drug metabolism and stress response, while not affecting those related to other drug pathways, thereby highlighting the specificity of AHR-mediated regulatory effects in this context (Figure S2g, Supplemental Digital Content 1, http://links.lww.com/MPA/B412).

AHR is essential for drug-induced but not basal expression of CYP2S1 in PDAC

To further dissect the mechanism of CYP2S1 induction, knockdown experiments were performed independently for AHR or CYP2S1 in PACO10 and PACO18 cells. Knockdown of AHR did neither impact the basal mRNA expression of CYP2S1 (Figure 5e) nor its protein expression (Figure S3a, Supplemental Digital Content 1,

http://links.lww.com/MPA/B412). However, AHR knockdown abolished the previously observed inducibility of CYP2S1 levels upon SN38 treatment in PACO cell lines (**Figure 5f**) as well as in CAPAN1 cells (Figure S3b, c, Supplemental Digital Content 1, http://links.lww.com/MPA/B412). These findings suggest that AHR mediates the SN38-induced but not the basal expression of CYP2S1 in PDAC.

## HNF4A is involved in basal expression of CYP2S1 in PDAC

It is known from literature that hepatocyte nuclear factors can act as transcription factors for CYP enzymes. Indeed, transient siRNA-based knockdown of HNF4A (hepatocyte nuclear factor 4 alpha), which is relevant for basal expression of CYP3A5, reduced basal levels of CYP2S1 expression in PACO10 and PACO18 cells (**Figures 5g**, S3d, Supplemental Digital Content 1, http://links.lww.com/MPA/B412), while treatment with SN38 still induced CYP2S1 upregulation (**Figure 5h**). We thus conclude that HNF4A is involved in basal but not in SN38-induced expression of CYP2S1. Indeed, increased endogenous expression of HNF4A protein was observed in the HNF1A+ PDAC subtype relative to the other subtypes or normal pancreas (Figure S3e, Supplemental Digital Content 1, http://links.lww.com/MPA/B412), as previously also shown in <sup>5</sup>.

Alterations of CYP2S1 or AHR levels influence the efficacy of SN38 in PACO cell lines

Since members of the CYP family are detoxification enzymes which transform many of their
ligands, it was hypothesized that CYP2S1 might functionalize and detoxify SN38, thereby
contributing to therapy resistance. To evaluate this hypothesis, CYP2S1 knockdown cell
lines, AHR knockdown cell lines and CYP2S1 overexpression cell lines were generated.

Consistent with the working hypothesis, both PACO18 and PACO10 cells showed a strong
and highly significant decrease in cell survival upon SN38 treatment, if either AHR or
CYP2S1 was subjected to knockdown (Figure. 6a).

Interestingly, for PACO18 this effect was even more pronounced for AHR knockdown, pointing towards an impact of AHR on SN38 detoxification beyond CYP2S1-induced clearance. For PACO18 the knockdown of CYP2S1 decreased the IC50 for SN38 by a factor of ~10 from 75.0 nM to 7.7 nM (Figure 6d, upper panel), while knockdown of AHR resulted in a ~22-fold decrease of the IC50 from 75.0 nM to 3.4 nM (**Figure 6c, upper** panel). A similar trend was observed for PACO10 cells upon CYP2S1 or AHR knockdown. For PACO10 the knockdown of CYP2S1 decreased the IC50 for SN38 by a factor of ~9 from 8.6 nM to 0.9 nM (Figure 6d, lower panel), while knockdown of AHR resulted in a ~10-fold decrease of the IC50 from 8 nM to ~ 0.8 nM (**Figure 6c, lower panel**). As expected based on the working hypothesis, transduction of PACO10 and PACO18 with a CYP2S1 overexpression vector inverted the picture in both cell lines: Upon overexpression of CYP2S1, PACO10 and PACO18 cells showed a significant better survival upon SN38 treatment, compared to the empty vector control (Figure 6b, Figure 6e). For PACO18, the cell line with the highest endogenous expression of CYP2S1, the IC50 of SN38 increased relative to the empty vector control by a factor of ~37 (4.8 nM to 178.2 nM), while an increase by a factor of ~56 (5.2 nM to 289.1 nM) was observed for PACO10. We further performed KD and OE experiments in CAPAN1 and PANC1 cell lines and in line with our previous results, while both KD and OE had similar effects in CAPAN1 cells compared to the PACO cells with the HNF1a subtype the HNF1a- PANC1 cells were less affected by KD and OE (Figure S3f, g, Supplemental Digital Content 1, http://links.lww.com/MPA/B412). These KD and OE effects were specific to SN-38 treatment and cell proliferation was not altered in the CYP2S1 KD, AHR KN or CYP2S1 OE upon treatment with drugs like paclitaxel and gemcitabine in PACO cells (Figure S4a-d, Supplemental Digital Content 1, http://links.lww.com/MPA/B412)

A further cell toxicity assay performed 24, 48 and 72 hours after SN38 treatment demonstrated a lower cell toxicity for PACO18 cells overexpressing CYP2S1 after 72 hours of SN38 treatment, but not before (Figure S4e, Supplemental Digital Content 1, http://links.lww.com/MPA/B412). Interestingly, differences in cell survival upon knockdown or overexpression were less pronounced or not significant for the KRT81+ subtype (Figure S4f, Supplemental Digital Content 1, http://links.lww.com/MPA/B412), which is characterized by low endogenous CYP2S1 and AHR levels (Figure S2d, Supplemental Digital Content 1, http://links.lww.com/MPA/B412). To evaluate whether PAH exposure can induce SN38 resistance we pre-treated PDAC cells with a low, non-toxic concentration of TCDD prior to SN38 treatment. The cells were exposed to TCDD for 2 days, after which the drug was removed and the cells were treated with SN38 for 4 days. Recognizing that CYP2S1 expression peaks after 2 days of SN38/TCDD treatment (see timeline of induction Fig3c, 5b) and subsequently declines, we performed an additional experiment. Cells were pre-treated with TCDD for 1 day, then allowed to recover in fresh medium for 2 days before being treated with SN38 for 3 days. Our results showed that a 2-day pre-treatment with TCDD led to a modest but statistically significant increase in cell viability following SN38 treatment. However, when cells were allowed to recover for 2 days after TCDD exposure before SN38 treatment, no additional TCDD-induced toxicity was observed, and there was no significant change in SN38 sensitivity compared to controls. In conclusion, pre-treatment with an AHR-activating agent such as TCDD effectively induces CYP2S1 expression and accelerates the metabolism of SN38, bypassing the typical 24-48-hour induction period. However, this effect is transient, and once the AHR ligand is removed, CYP2S1 levels decrease, resulting in no sustained survival benefit against SN38 toxicity (Figure S4h, i, Supplemental Digital Content 1, http://links.lww.com/MPA/B412).

#### **Discussion**

The absence of early symptoms in PDAC usually prevents timely diagnosis before metastasis precludes surgical resection and treatment with curative intent. Deepening the understanding of the proteogenomic differences between the PDAC subtypes is one possibility to tailor medical strategies for an improved therapeutic outcome. Here we provide in-depth proteomic profiles for the different PDAC subtypes previously proposed based on gene expression and surrogate markers by Collison, Noll and Espinet <sup>4,5,29,30</sup>. Of note, while the initially reported ADEX subtype might have been the result of contamination of normal cells (doi: 10.1053/j.gastro.2018.08.033.), our cell lines have been verified to be pure PDAC cell lines (Noll et al.)

While Noll *et al.* have described the functional importance of cell-autonomous drug detoxification mediated by CYP3A5, <sup>5</sup> our data complement these findings with the observation that CYP3A5 is not the only player contributing to drug resistance in the HNF1A+ PDAC subtype. By large-scale proteomics analysis, a broad set of detoxification enzymes including AKR1B10, CES2, CYP2S1, GPX2, GSR, HNMT, MAOB, UGT1A10 and UGT1A6 was found upregulated in the HNF1A+ PDAC subtype. While further research is required to unravel the specific impact and mode of action for each of these proteins in the context of PDAC, we have selected CYP2S1 for further functional studies based on its particularly consistent and high expression differences, and the known role of CYPs in drug detoxification.

The HNF1A+ PDAC subtype showed the highest expression of CYP2S1, whereas the KRT81+ subtype was characterized by lower CYP2S1 protein levels. Identified by Rylander *et al.*, <sup>31</sup> CYP2S1 is one of the less well characterized "orphan" members of the cytochrome P450 monooxygenase family, but has been described to be involved in the metabolism of endogenous retinoids, eicosanoids and dioxin <sup>25, 32, 33</sup>. At least in some tissues and/or species, CYP2S1 can be induced by dioxin via AHR and ARNT <sup>25, 32</sup>. In mice, Rivera *et al.* have

reported that a regulatory cassette mediates changes in CYP2S1 expression via XRE sequences binding AHR/ARNT dimer in a dioxin-dependent fashion in vitro 34. We could confirm that various polyaromatic hydrocarbons including 2,3,7,8tetrachlorodibenzo-p-dioxin, benzo(a)pyrene, β-naphthoflavone and 3-methylcholanthrene alter the expression profile of the AHR target gene TIPARP and also of CYP2S1 in human PDAC cell lines. In addition to the induction by these classical carcinogenic PAHs, we furthermore uncovered the potent induction of CYP2S1 by the topoisomerase inhibitor SN38 and its analogue topotecan in cell lines of the HNF1A+ or KRT81+ PDAC subtypes. Where a drug is capable of increasing transcription and/or translation of specific CYPs, these CYPs are often the most efficient metabolizers of that chemical <sup>35</sup>. Indeed, our data demonstrate that overexpression of CYP2S1 improved the survival of pancreatic cancer cell lines of the HNF1A+ subtype upon treatment with SN38. Vice versa, knockdown of CYP2S1 in these PACO cells resulted in a significant decrease in cell survival upon treatment, suggesting that the absence of CYP2S1 sensitizes these tumor cells to SN38 and indicating that CYP2S1 plays a key role in the SN38 detoxification process in HNF1A+ PDAC cells. However, depending on the respective subtype, further enzymes might be involved in the multi-step detoxification cascade: In a cell line of a different subtype, overexpression of CYP2S1 was not sufficient to reduce efficacy of SN38.

Tobacco smoke and consumption of smoked/grilled foods are usually the dominant sources of human exposition to PAHs. Both variables are listed as risk factors for the development of pancreatic cancer, and tobacco use in the form of cigarette or cigar smoking even doubles the risk for pancreatic cancer <sup>36</sup>. It might be interesting to analyse, if smoking can induce CYP2S1 expression and may thereby affect the therapeutic window for irinotecan, topotecan, SN38 or further drugs with a PAH-like structure, at least in certain cancer (sub)types.

A significant improvement for patients with metastatic PDAC was achieved in 2011, when the ACCORD trial introduced the FOLFIRINOX regimen (folinic acid, fluorouracil, irinotecan and oxaliplatin) as a new and effective treatment for PDAC <sup>3, 37</sup>. Because irinotecan is used as part of the FOLFIRINOX scheme, accelerating the pharmacokinetics of its active metabolite SN38 by induced AHR or CYP2S1 expression might shift the therapeutic window of the treatment and impact the therapeutic response. In view of the findings presented herein we suggest incorporating AHR and CYP2S1 as variables in pharmacokinetic modelling for drug development and dose finding to improve the accuracy for predicting the optimal conditions for therapies comprising irinotecan, SN38 or topotecan. Furthermore, we could show that the expression of AHR is crucial for CYP2S1 induction in PDAC. Knockdown of AHR decreased cell survival in PACO cells, but did not affect intrinsic CYP2S1 expression. This suggests that AHR contributes to drug-induced CYP2S1 expression while basal expression of CYP2S1 is mediated by different transcription factors. Since CYP2S1 expression is dispensable for the normal growth of cells, its inhibition is a promising therapeutic option for cancer treatment or co-treatment with irinotecan, SN38 or topotecan. The described CYP2S1 or AHR mediated resistance mechanism is most likely not limited to PDAC, since both proteins are also expressed in other cancer types, including colorectal cancer. Irinotecan has obtained regulatory approval not only for PDAC but also for metastatic colorectal cancer, while topotecan is used to treat e.g., ovarian cancer and lung cancer. Consequently, the CYP2S1/AHR mechanism could also be of importance for drug pharmacokinetics and treatment resistance in these cancer types.

In summary, this large-scale proteomic analysis contributes to a better understanding of the subtype-specific detoxification mechanisms in PDAC. Blocking AHR or CYP2S1 either alone or in combination, e.g., by small molecule inhibitors, might provide a path to suppress CYP2S1 mediated resistance to chemotherapy.

Acknowledgments We are indebted to our friend and colleague Wilko Weichert, who tragically passed away during preparation of this manuscript. It was an honor and pleasure to work with Wilko, who inspired us with his great passion for science. We acknowledge kind support by Edward Green for setting up the AHR-ligand assay. We thank Marion Mielke (CEP, Institute of Pathology, TUM) for excellent technical support and we thank the members of the Central Animal Laboratory at DKFZ for animal husbandry.

**Data Availability:** All quantification data generated in this study are available within the article and its supplementary data files. Additional raw data are available upon request.

Author Contributions: WMN and CR conceived and planned and WMN performed all mass spectrometric experiments. AK and CR developed the quantification software suites around MSQBAT. LK provided support for cell culturing / mass spectrometric maintenance. WMN found the differential regulation of various biotransformation proteins including CYP2S1 and suggested the relevance of CYP2S1 for detoxification in PDAC subtypes. WMN and VT suggested, designed and performed all associated functional experiments and wrote the manuscript. VT suggested and performed the AHR-ligand assay. CK and VV performed the experiments for Fig. 2c. NAG, TH, RK, HYY, KS and WW curated patient cohorts, handled patient specimens and contributed the results shown in Fig. S3, Supplemental Digital Content 1, http://links.lww.com/MPA/B412. MRS, VT and EN suggested the relevance of HNF4A for CYP2S1 expression and VT performed the associated experiments. MRS, CR, AT CAO, MR, and LK provided valuable scientific input and contributed in discussions. VT performed all experiments for revision with support from TV and PSK. All authors have read and reviewed the manuscript.

#### References

- 1. Tonini V, Zanni M. Pancreatic cancer in 2021: What you need to know to win. *World J Gastroenterol*. 2021;27(35):5851.
- 2. Kanji ZS, Gallinger S. Diagnosis and management of pancreatic cancer. *Can Med Assoc J.* 2013;185(14):1219-1226.
- 3. Conroy T, Hammel P, Hebbar M, et al. FOLFIRINOX or gemcitabine as adjuvant therapy for pancreatic cancer. *N Engl J Med*. 2018;379(25):2395-2406.
- 4. Collisson EA, Sadanandam A, Olson P, et al. Subtypes of pancreatic ductal adenocarcinoma and their differing responses to therapy. *Nat Med*. 2011;17(4):500-503.
- 5. Noll EM, Eisen C, Stenzinger A, et al. CYP3A5 mediates basal and acquired therapy resistance in different subtypes of pancreatic ductal adenocarcinoma. *Nat Med*. 2016;22(3):278-287.
- 6. Xu Z, Hu K, Bailey P, et al. Clinical Impact of Molecular Subtyping of Pancreatic Cancer. *Front cell Dev Biol*. 2021;9.
- 7. Conroy T, Hammel P, Hebbar M, et al. Canadian Cancer Trials Group and the Unicancer-GI–PRODIGE Group. *FOLFIRINOX or gemcitabine as Adjuv Ther Pancreat cancer N Engl J Med*. 2018;379(25):2395-2406.
- 8. Bailey P, Chang DK, Nones K, et al. Genomic analyses identify molecular subtypes of pancreatic cancer. *Nature*. 2016;531(7592):47-52.
- 9. Moffitt RA, Marayati R, Flate EL, et al. Virtual microdissection identifies distinct

tumor-and stroma-specific subtypes of pancreatic ductal adenocarcinoma. *Nat Genet*. 2015;47(10):1168.

- 10. Cao L, Huang C, Zhou DC, et al. Proteogenomic characterization of pancreatic ductal adenocarcinoma. *Cell.* 2021;184(19):5031-5052.
- 11. Network CGAR. Raphael, BJ Integrated genomic characterization of pancreatic ductal adenocarcinoma the cancer genome atlas research network. *Cancer Cell*. 2017;32:185-203.
- 12. Pan S, Brentnall TA, Chen R. Proteome alterations in pancreatic ductal adenocarcinoma. *Cancer Lett.* 2020;469:429-436.
- 13. Long J, Zhang Y, Yu X, et al. Overcoming drug resistance in pancreatic cancer. Expert Opin Ther Targets. 2011;15(7):817-828.
- 14. Anzenbacher P, Anzenbacherová E. Cytochromes P450 and metabolism of xenobiotics. *Cell Mol Life Sci.* 2001;58(5):737-747.
- 15. Kumarakulasingham M, Rooney PH, Dundas SR, et al. Cytochrome p450 profile of colorectal cancer: identification of markers of prognosis. *Clin Cancer Res.* 2005;11(10):3758-3765.
- 16. Li Y, Su X, Feng C, et al. CYP2S1 is a synthetic lethal target in BRAFV600E-driven thyroid cancers. *Signal Transduct Target Ther*. 2020;5(1):1-12.
- 17. Kawato Y, Aonouma M, Matsumoto K, Sato K. Production of SN-38, a main metabolite of the camptothecin derivative CPT-11, and its species and tissue specificities.

  \*Drug Metab Pharmacokinet. 1991;6(6):899-907.

- 18. Minami H, Sai K, Saeki M, et al. Irinotecan pharmacokinetics/pharmacodynamics and UGT1A genetic polymorphisms in Japanese: roles of UGT1A1\* 6 and\* 28. *Pharmacogenet Genomics*. 2007;17(7):497-504.
- 19. Lee KM, Nguyen C, Ulrich AB, Pour PM, Ouellette MM. Immortalization with telomerase of the Nestin-positive cells of the human pancreas. *Biochem Biophys Res Commun.* 2003;301(4):1038-1044.
- 20. Furukawa T, Duguid WP, Rosenberg L, Viallet J, Galloway DA, Tsao M-S. Long-term culture and immortalization of epithelial cells from normal adult human pancreatic ducts transfected by the E6E7 gene of human papilloma virus 16. *Am J Pathol*. 1996;148(6):1763.
- 21. Muckenhuber A, Berger AK, Schlitter AM, et al. Pancreatic ductal adenocarcinoma subtyping using the biomarkers hepatocyte nuclear factor-1A and cytokeratin-81 correlates with outcome and treatment response. *Clin Cancer Res.* 2018;24(2):351-359.
- 22. Alexander Kerner. MSqBAT Software. https://sourceforge.net/projects/msqbat/.
- 23. Szklarczyk D, Franceschini A, Wyder S, et al. STRING v10: protein—protein interaction networks, integrated over the tree of life. *Nucleic Acids Res.* 2015;43(D1):D447-D452.
- 24. Pieter Giesbertz, Denise Slenter, Kristina Hanspers; Daniela Digles et al. Wikipathways. https://www.wikipathways.org/index.php/Pathway:WP702.
- 25. Rivera SP, Saarikoski ST, Hankinson O. Identification of a novel dioxin-inducible cytochrome P450. *Mol Pharmacol*. 2002;61(2):255-259.
- 26. Murray IA, Patterson AD, Perdew GH. Aryl hydrocarbon receptor ligands in cancer:

friend and foe. Nat Rev Cancer. 2014;14(12):801-814.

- 27. Watson JD, Prokopec SD, Smith AB, Okey AB, Pohjanvirta R, Boutros PC. TCDD dysregulation of 13 AHR-target genes in rat liver. *Toxicol Appl Pharmacol*. 2014;274(3):445-454.
- 28. Kunimoto T, Nitta K, Tanaka T, et al. Antitumor activity of 7-ethyl-10-[4-(1-piperidino)-1-piperidino] carbonyloxycamptothecin, a novel water-soluble derivative of camptothecin, against murine tumors. *Cancer Res.* 1987;47(22):5944-5947.
- 29. Kuhlmann L, Nadler WM, Kerner A, et al. Identification and validation of novel subtype-specific protein biomarkers in pancreatic ductal adenocarcinoma. *Pancreas*. 2017;46(3):311-322.
- 30. Espinet E, Gu Z, Imbusch CD, et al. Aggressive PDACs Show Hypomethylation of Repetitive Elements and the Execution of an Intrinsic IFN Program Linked to a Ductal Cell of Origin. *Cancer Discov.* 2021;11(3):638-659.
- 31. Rylander T, Neve EPA, Ingelman-Sundberg M, Oscarson M. Identification and tissue distribution of the novel human cytochrome P450 2S1 (CYP2S1). *Biochem Biophys Res Commun.* 2001;281(2):529-535.
- 32. Saarikoski ST, Rivera SP, Hankinson O, Husgafvel-Pursiainen K. CYP2S1: a short review. *Toxicol Appl Pharmacol*. 2005;207(2):62-69.
- 33. Bui P, Imaizumi S, Beedanagari SR, Reddy ST, Hankinson O. Human CYP2S1 metabolizes cyclooxygenase-and lipoxygenase-derived eicosanoids. *Drug Metab Dispos*. 2011;39(2):180-190.

- 34. Rivera SP, Wang F, Saarikoski ST, et al. A novel promoter element containing multiple overlapping xenobiotic and hypoxia response elements mediates induction of cytochrome P4502S1 by both dioxin and hypoxia. *J Biol Chem.* 2007;282(15):10881-10893.
- 35. Coleman MD. Human Drug Metabolism. John Wiley & Sons; 2020.
- 36. Seufferlein T, Porzner M, Becker T, et al. S3-Leitlinie zum exokrinen Pankreaskarzinom. *Z Gastroenterol*. 2013;51(12):1395-1440.
- 37. Conroy T, Desseigne F, Ychou M, et al. FOLFIRINOX versus gemcitabine for metastatic pancreatic cancer. *N Engl J Med*. 2011;364(19):1817-1825.

Figure 1. Proteomic analysis of PDAC subtypes. (a) Workflow of the quantitative GeLCbased MALDI/MS analysis of twelve human PDAC cell lines and two control cell lines. (b) Principal component analysis based on the glog2-transformed intensities of the 500 most variable proteins quantified in the PACO and control cell lines using MSQBAT. (c) Numbers of proteins with differential expression between at least two subtypes/groups. Differential expression was assessed using linear models and was considered significant for proteins with a BH adjusted p value < 0.05. The respective subtype annotation for each cell line is provided in Table S1b, Supplemental Digital Content 2, http://links.lww.com/MPA/B413. (d) STRING protein/protein interaction analysis using the resulting 310 proteins with significant differential expression between at least two subtypes/groups as input, section from overview image as shown in Figure S1, Supplemental Digital Content 1, http://links.lww.com/MPA/B412. Enrichment analysis revealed significant functional enrichment, inter alia for gene ontology terms capturing oxidation-reduction processes (red, FDR = 3.07e-06), small molecule metabolic processes (blue, FDR = 3.07e-06), and metabolic

processes (green, FDR = 3.07e-06).

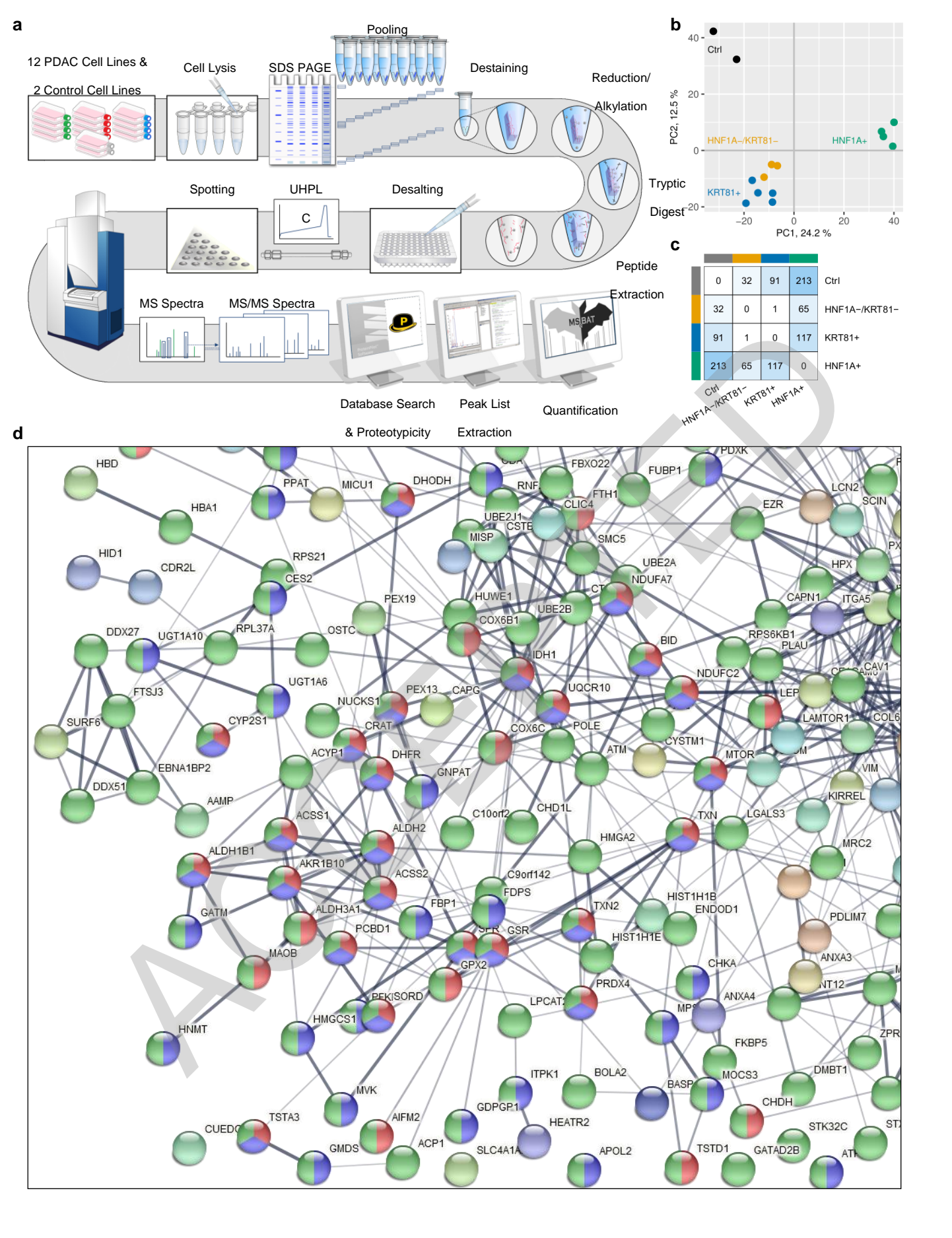


Figure 2. Biotransformation-related proteins in PDAC subtypes (a) Metapathway biotransformation with heatmaps of proteins with known involvement in detoxification processes as quantified using in-house software MSQBAT. Ratios were computed as row z score based on glog2 transformed intensities. γ-EC: γ-glutamylcysteine, G: glycine, SG: glutathione, Ac: acetyl group, Gl: glucuronic acid. (b) MRM-quantified protein levels of selected biotransformation enzymes in human pancreas samples, human liver samples, or HNF1A+ PDAC cell lines PACO10, PACO14, and PACO18, normalized by total protein. (c) Immunohistochemistry of HNF1A+ PACO14 and PACO18 mouse xenograft sections showing CYP2S1 and AHR endogenous expression. Scale bar: 100 µm. (d) AHR expression levels quantfied in PDAC or control cell lines HPDE/HPNE with MSQBAT. Ordinary oneway ANOVA with multiple comparisons with Dunnett's correction relative to the HNF1A+ subtype, \*/\*\*: adj. p < 0.05/0.01. (e) MRM-based validation of CYP2S1 expression levels in PDAC cell lines compared to normal pancreatic and liver samples. Log2-transformed ratios were computed relative to the average of the PACO cell lines. Mean  $\pm$  SD. Ordinary one-way ANOVA with multiple comparisons with Dunnett's correction, \*\*/\*\*\*: adj. p < 0.01/0.001/0.0001.

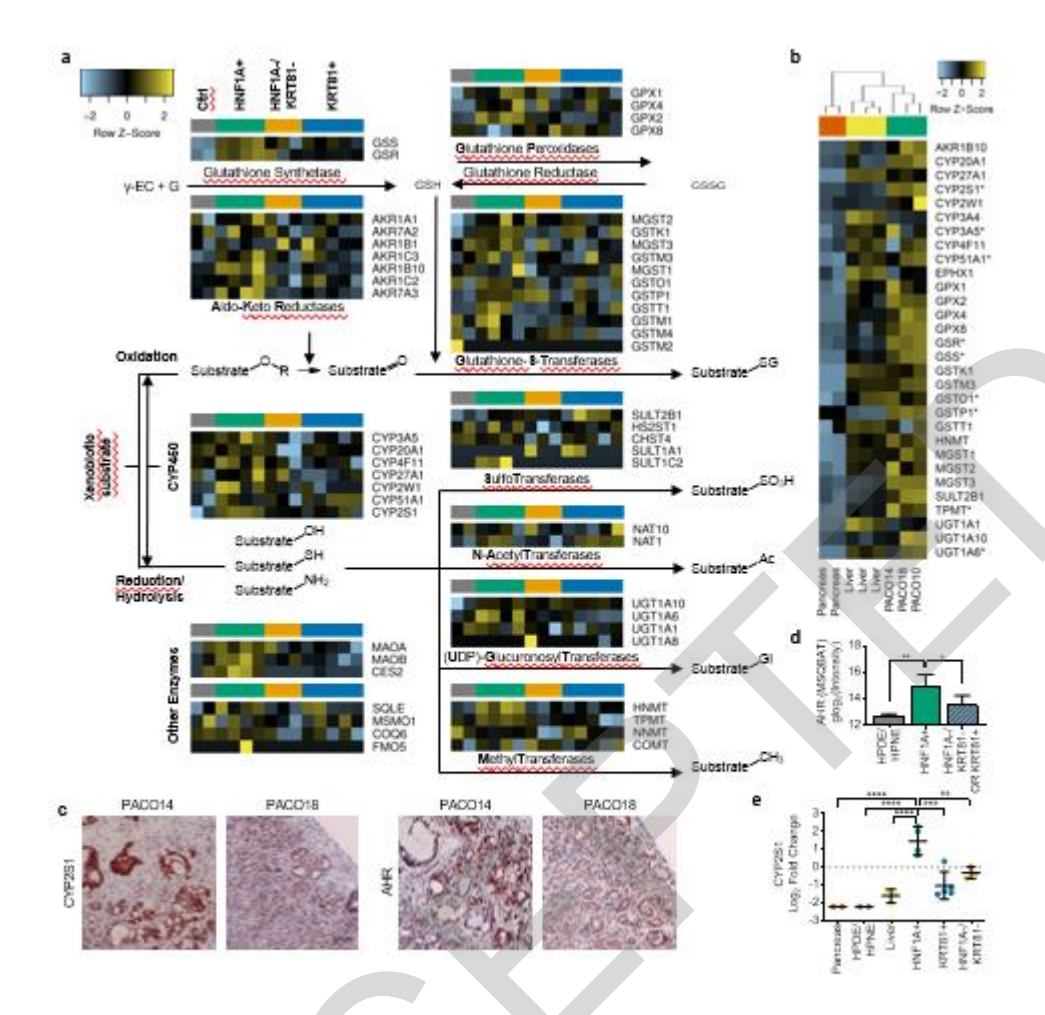


Figure 3. CYP2S1 induction in PDAC (a) TIPARP and CYP2S1 mRNA expression in response to TCDD (1 μM, 72 h) in HNF1A+ PDAC cell lines. Control: DMSO. n = 3, mean  $\pm$  SD. Multiple t tests with Holm-Sidak method, \*\*/\*\*\*: adj. p < 0.01/0.001. (b) Timedependent induction of TIPARP and CYP2S1 mRNA expression upon TCDD treatment (1 μM) in HNF1A+ cell line PACO18. The mRNA levels were calculated relative to DMSO control. n = 3, mean  $\pm$  SD. (c) TIPARP and CYP2S1 mRNA expression in response to different PAHs (10 µM, 72 h) in HNF1A+ cell line PACO 10. Control: DMSO. Mean ± SD. Multiple t tests with Holm-Sidak method, \*/\*\*: adj. p < 0.05/0.01. (d) Chemical structures of PAHs acting as inducers of AHR target gene TIPARP and CYP2S1. (e) Confocal microscopy images showing increased AHR expression/nuclear translocation in HNF1A+ PDAC cell line PACO18 after exposure to TCDD (1 µM, 72 h) or BaP (10 µM, 72 h). Co-treatment of the cells with BaP (10 µM) and AHR inhibitor (AHRi, SR 182706, Merck Millipore, 1 µM) for 72 h was used as control and indicated lower total levels of AHR without specific nuclear accumulation.

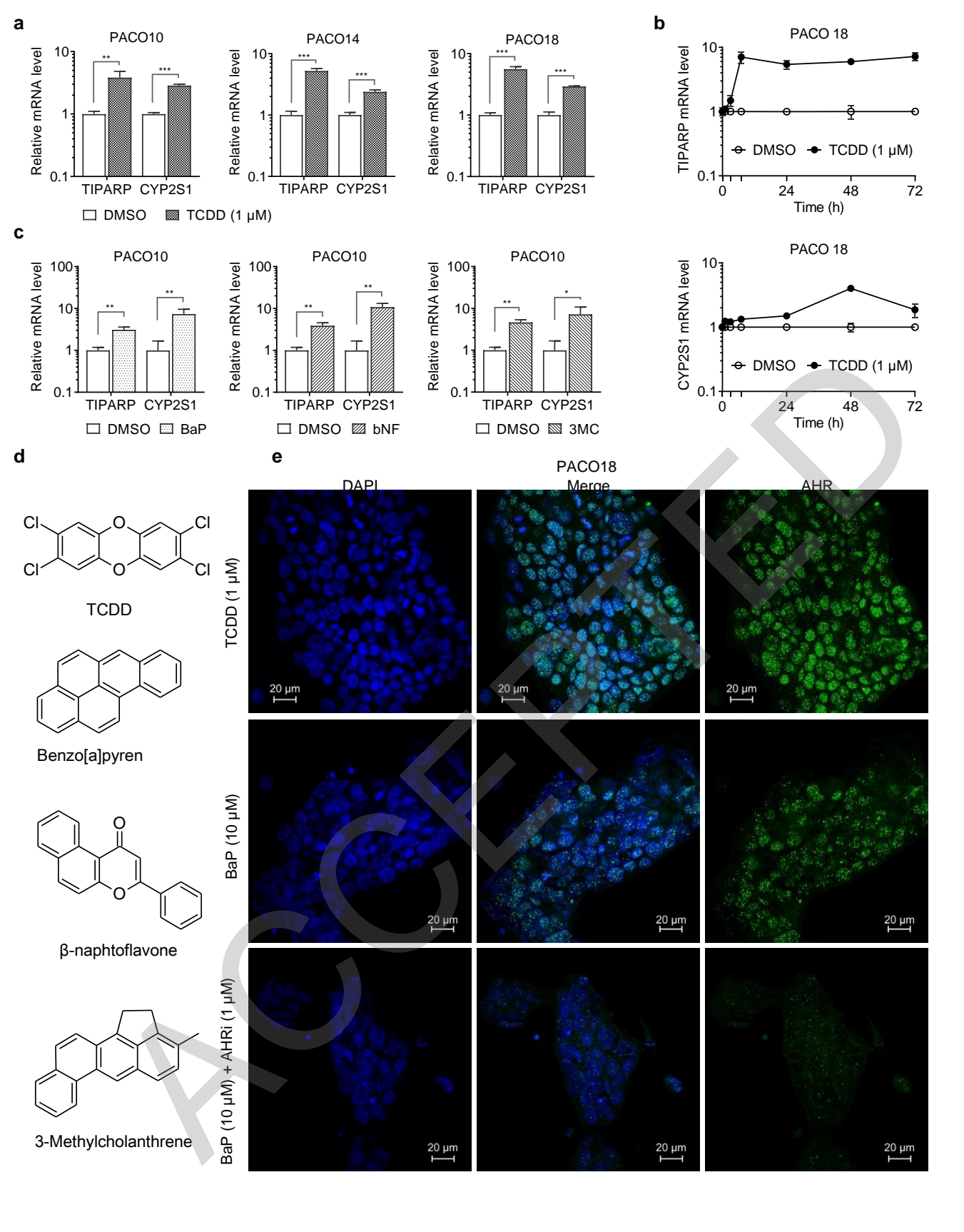


Figure 4. Confocal microscopy images showing CYP2S1 protein expression in HNF1A+ PDAC cell line PACO14 after exposure to AHR inhibitor (AHRi, SR 182706, Merck Millipore, 1  $\mu$ M, 72 h), BaP (10  $\mu$ M, 72 h), or simultaneous treatment with both compounds.

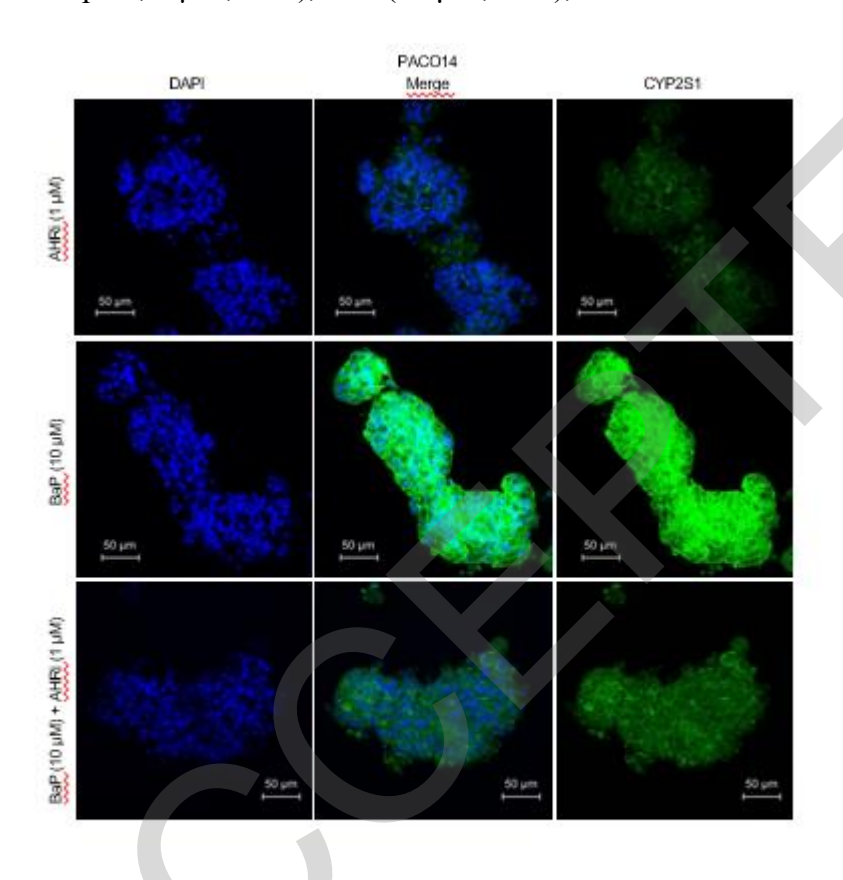


Figure 5. Relevance of SN38 for CYP2S1 induction (a) TIPARP and CYP2S1 mRNA expression in response to SN38 treatment (1 µM, 72 h) in different PDAC cell lines (48 h for PACO 7). Control: DMSO. n = 3, mean  $\pm$  SD. Multiple t tests with Holm-Sidak method, \*/\*\*/\*\*: adj. p < 0.05/0.01/0.001. (b) Time-dependent induction of TIPARP and CYP2S1 mRNA expression upon SN38 treatment (1 µM) in HNF1A+ PDAC cell line PACO18. The mRNA levels were calculated relative to DMSO control. Mean ± SD. (c) AHR-ligand assay using HEK293T cells transfected with the Cignal AHR-GFP Reporter Assay or negative control. Fluorescence after treatment with vehicle control (PBS), positive control (dARNT) or SN38 (1  $\mu$ M) for 24 h. Increased fluorescence indicates successful binding to AHR. n = 3, mean  $\pm$  SD. Unpaired t test,\*\*\*\*: p < 0.0001. (d) TIPARP and CYP2S1 mRNA expression after treatment of HNF1A+ PDAC cells with SN38 analog topotecan (1 µM, 72 h). Control: DMSO. n = 3, mean  $\pm$  SD. Multiple t tests with Holm-Sidak method, \*\*\*: adj. p < 0.001. (e) Impact of AHR knockdown (KD) on basal mRNA levels of AHR and CYP2S1. n = 3, mean ± SD. Multiple t tests with Holm-Sidak method, \*: adj. p < 0.05. No significant reduction of CYP2S1 level is observed. (f) CYP2S1 mRNA expression after treatment with DMSO control or SN38 (1 µM, 72 h) in two HNF1A+ PDAC cell lines w/o (NT) or with AHR knockdown (AHR KD). Controls: non-targeting (NT), DMSO. n = 3, mean  $\pm$  SD. Multiple t tests with Holm-Sidak method, \*\*/\*\*\*: adj. p < 0.01/0.001. Knockdown of AHR impairs inducibility of CYP2S1 by SN38 in PDAC cells. (g) Impact of transient HNF4A knockdown on relative HNF4A or CYP2S1 mRNA expression in HNF1A+ PACO10. Control: nontargeting (NT). n=3, mean  $\pm$  SD. Multiple t tests with Holm-Sidak method, \*\*: adj. p<0.01. (h) Relative CYP2S1 mRNA expression after treatment with DMSO control or SN38 (1  $\mu$ M, 72 h) in two HNF1A+ PDAC cell lines with (siHNF4A) or w/o (siNT) transient HNF4A knockdown. Controls: non-targeting (siNT), DMSO. n=3, mean  $\pm$  SD. Multiple t tests with Holm-Sidak method, \*\*/\*\*\*: adj. p<0.01/0.001.

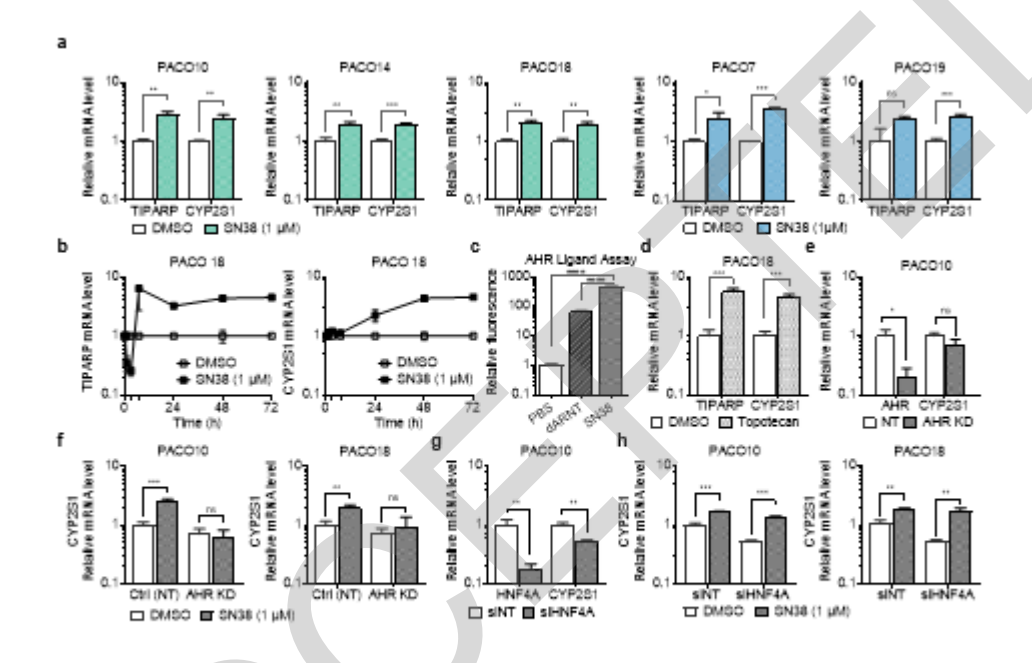


Figure 6. Impact of CYP2S1/AHR levels on cell viability after treatment with SN38 (a), (b) Cell viability after treatment with 100 nM SN38 (72 h) for two HNF1A+ PDAC cell lines with or w/o (a) knockdown of CYP2S1 or AHR, or (b) overexpression of CYP2S1. n = 12 (4 biological x 3 technical replicates), mean  $\pm$  SD. Unpaired t-test, \*\*\*\*: p < 0.0001. (c), (d) Dose response curves showing the cell viability after treatment with SN38 (72 h) for two HNF1A+ PDAC cell lines with (KD) or w/o (NT) knockdown of (c) AHR or (d) CYP2S1. Control: DMSO, n = 4, mean  $\pm$  SD. RM Two way ANOVA with Geisser-Greenhouse correction. Knockdown of AHR or CYP2S1 significantly sensitized the PDAC cell lines to SN38 (AHR: p < 0.0007 for PACO18 / p < 0.0008 for PACO10; CYP2S1: p < 0.0002 for PACO18 / p < 0.0018 for PACO10). (e) Dose response curves showing the cell viability after treatment with SN38 (72 h) for two HNF1A+ PDAC cell lines with (CYP2S1 OE) or w/o (CYP2S1 EV) overexpression of CYP2S1. Control: DMSO, n = 4, mean  $\pm$  SD. Mixed-effects analysis was used for PACO18 to account for missing values. Fixed effects were observed for CYP2S1 overexpression (p < 0.0001). RM Two way ANOVA with Geisser-Greenhouse correction was used for PACO10. Overexpression of CYP2S1 significantly increased the resistence of the PDAC cell lines to SN38 (PACO18: p < 0.0001 / PACO10: p < 0.0096). IC50 values were calculated using a nonlinear fit with variable slope (four parameters) and least squares regression.

